Author(s): Ren, Liting; Yuan, Peng; Su, Haifeng; Malola, Sami; Lin, Shuichao; Tang, Zichao; Teo, Boon K.; Häkkinen, Hannu; Zheng, Lansun; Zheng, Nanfeng

Title: Bulky Surface Ligands Promote Surface Reactivities of [Ag141X12(S-Adm)40]3+ (X=Cl, Br, I) Nanoclusters: Models for Multiple-Twinned Nanoparticles

Year: 2017

Version:

Please cite the original version:

Ren, L., Yuan, P., Su, H., Malola, S., Lin, S., Tang, Z., Teo, B. K., Häkkinen, H., Zheng, L., & Zheng, N. (2017). Bulky Surface Ligands Promote Surface Reactivities of [Ag141X12(S-Adm)40]3+ (X=Cl, Br, I) Nanoclusters: Models for Multiple-Twinned Nanoparticles. Journal of the American Chemical Society, 139(38), 13288-13291. https://doi.org/10.1021/jacs.7b07926

Communication

Bulky Surface Ligands Promote Surface Reactivities of [Ag141X12(S-Adm)40]3+ (X=Cl, Br, I) Nanoclusters: Models for Multiple-Twinned Nanoparticles

Liting Ren, peng yuan, Hai-Feng Su, Sami Malola, Shui-Chao Lin, Zichao Tang, Boon K. Teo, Hannu Häkkinen, Lan-Sun Zheng, and Nanfeng Zheng

J. Am. Chem. Soc., **Just Accepted Manuscript** • DOI: 10.1021/jacs.7b07926 • Publication Date (Web): 11 Sep 2017

Bulky Surface Ligands Promote Surface Reactivities of $[Ag_{141}X_{12}(S\text{-}Adm)_{40}]^{3+}$ (X=Cl, Br, I) Nanoclusters: Models for Multiple-Twinned Nanoparticles

Liting Ren,[1§] Peng Yuan,[1§] Haifeng Su,[1] Sami Malola,[2] Shuichao Lin,[1] Zichao Tang,[1] Boon K. Teo,[1,*] Hannu Häkkinen,[2,*] Lansun Zheng,[1] Nanfeng Zheng[1,*]

[1] Collaborative Innovation Center of Chemistry for Energy Materials, State Key Laboratory for Physical Chemistry of Solid Surfaces, and Department of Chemistry, College of Chemistry and Chemical Engineering, Xiamen University, Xiamen 361005, China
[2] Departments of Physics and Chemistry, Nanoscience Center, University of Jyväskylä, FI-40014 Jyväskylä, Finland

Supporting Information

ABSTRACT: Surface ligands play important roles in controlling the size and shape of metal nanoparticles and their surface properties. In this work, we demonstrate that the use of bulky thiolate ligands, along with halides, as the surface capping agent promotes the formation of plasmonic multiple-twinned Ag nanoparticles with high surface reactivities. The title nanocluster $[Ag_{141}X_{12}(S\text{-}Adm)_{40}]^{3+}$ (where X = Cl, Br, I; S-Adm=1-adamantanethiolate) has a multiple-shell structure with an Ag_{71} core protected by a shell of $Ag_{70}X_{12}(S\text{-}Adm)_{40}$. The Ag_{71} core can be considered as twenty frequency-two Ag_{10} tetrahedra fused together with a dislocation that resembles multiple-twinning in nanoparticles. The nanocluster has a strong plasmonic absorption band at 460 nm. Due to the bulkiness of S-Adm, the nanocluster has a low surface thiolate coverage and thus unusually high surface reactivities towards exchange reactions with different ligands, including halides, phenylacetylene and thiols. The cluster can be made water soluble by metathesis with water-soluble thiols, thereby creating new functionalities for potential bioapplications.

Organic ligand stabilized metal nanoparticles have attracted much attention in the past two decades, owing to their unique properties.[1,2] Surface-capping agents play important roles, not only in stabilizing metal nanoparticles from aggregation, but also in controlling their size, shape, and morphology.[2-5] Many recent studies have also demonstrated that surface ligands on metal nanoparticles are capable of inducing steric and electronic effects that modify their catalytic properties.[6-11] However, due to the lack of effective techniques to characterize the binding structure of ligands on metal nanoparticles, it remains a challenge to understand how surface ligands facilitate the shape-controlled synthesis of metal nanoparticles. The latter is key to the ultimate manipulation of their surface properties. It is only through systematic studies of the structures and properties of a series of atomically precise metal clusters that new insights can be gained on how to control the size and morphology of nanoparticles.[12-19] For example, the combined use of phosphine and thiolate ligands was shown to facilitate the formation of cube-shaped Ag nanoparticles.[20,21]

Moreover, atomically precise metal nanoparticles have been successfully used as model catalysts to study the promotional effect of surface ligands on metal nanoparticles' catalysis.[22] However, basic understanding on how surface ligands dictate the morphology of a particular metal nanoparticle and its surface reactivity remains limited. In this work, we demonstrate that the use of bulky thiolates facilitates the formation of multiple-twinned Ag nanoparticles with enhanced surface reactivity. Specifically, with 1-adamantanethiolate and halide as surface ligands, Ag nanoparticles, $[Ag_{141}X_{12}(S\text{-}Adm)_{40}]^{3+}$(X = Cl, Br, I; S-Adm = 1-adamantanethiolate), were prepared. These nanoparticles have a multiple-twinned Ag_{71} core protected by a shell of $Ag_{70}X_{12}(S\text{-}Adm)_{40}$. The low surface coverage of thiolates on $[Ag_{141}X_{12}(S\text{-}Adm)_{40}]^{3+}$ caused by the sterically demanding S-Adm creates an unexpected enhancement of surface reactivity towards exchange reactions with halides, phenylacetylene and thiols. The clusters are thus easily converted into water-soluble Ag nanoparticles.

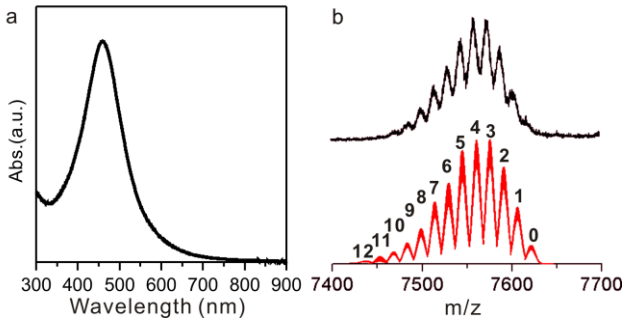

Figure 1. (a) UV-Vis spectrum of **1** in CH_2Cl_2. (b) ESI-MS spectra of the crude product of **1**, $[Ag_{141}Br_{12-n}Cl_n(S\text{-}Adm)_{40}]^{3+}$ (n=0-12).

The title nanoparticles were prepared by adopting a modified synthesis process of Ag_{136} and Ag_{374}.[18] For a typical synthesis of $[Ag_{141}Br_{12}(S\text{-}Adm)_{40}]^{3+}$ (**1**), a polymeric silver 1-adamantanethiolate was used as the metal precursor and reduced with $NaBH_4$ in the presence of PPh_4Br and triethylamine (see Supporting Information for details). The resulting Ag nanoparticles exhibited a strong UV-vis absorption band at 460 nm (Figure 1a), similar to the surface plasmon band of metallic Ag nanoparticles. The nanoparticles dissolved in CH_2Cl_2 were subjected to electrospray ionization mass spectrometry (ESI-MS). The multiple peaks between 7450 and 7650 (Figure 1b) can be assigned to an admixture of $[Ag_{141}Br_{12-n}Cl_n(S\text{-}Adm)_{40}]^{3+}$ with n = 0-12 with the isotopic pattern matched with the simulation (Figure S1).

High-quality dark green crystals were obtained by placing a dichloromethane solution in a closed container with toluene to slow down the crystallization process. **1** crystallizes in an orthorhombic space group *Pbcn* (Figure S2). The counter anions which could be halides were not identified due to disorder. Nevertheless, these nanoclusters were determined to

be trications by ESI-MS. The partial substitution of bromide by chloride is believed to be induced by the ESI-MS conditions. Including the ligand shell, **1** has a van der Waals diameter of about 3.0 nm with a metal core diameter of about 1.7 nm (Figure S3).

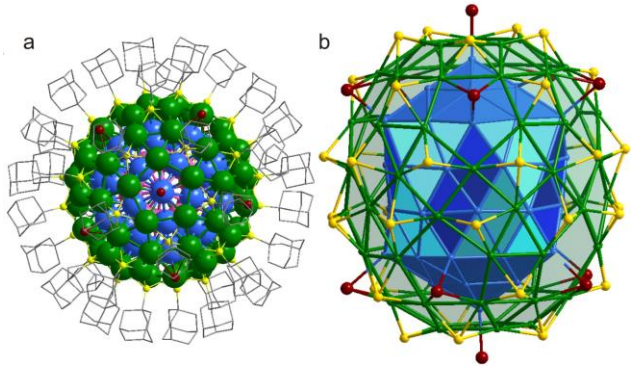

Figure 2. Overall structure of $[Ag_{141}Br_{12}(S\text{-}Adm)_{40}]^{3+}$ (characterized by X-ray crystallography) is viewed approximately along the fivefold (a) and twofold (b) symmetry axes. Green, blue, orange: silver; claret-red: bromide; yellow: sulfur; gray: carbon. All hydrogen atoms are omitted for clarity.

1 can be structurally described as a multiple-twinned Ag_{71} core terminated by a Ag-thiolate shell of $Ag_{70}(S\text{-}Adm)_{40}$ and 12 halides (Figure 2b). The ellipsoidal-shaped core consists of a two-shell $Ag_{19}@Ag_{52}$ structure (Figure 3a). The innermost shell is an interpenetrating biicosahedra (*IBI*) of Ag_{19} with two icosahedral centers bonded at 2.678 Å. The 17 peripheral atoms in the *IBI* form 30 triangles. Unlike many other known *IBIs*,[22] this *IBI* is twisted about the fivefold axis by 7.3 degrees. As a result, the point-group symmetry of the *IBI* core of **1** is lowered from D_{5h} to D_5, making it chiral (Figure S4). The overall structure of the Ag_{71} core can be described as 20 frequency-two (ν_2) tetrahedra interlaced together to form a multiple-twinned prolate metal core with 10 slightly concave butterfly "defects" (see the 20 dark blue triangles in the equator of Figure 3c). This unique interlacing configuration of 20 tetrahedra is observed for the first time. It suggests that 20 ν_2 *fcc* tetrahedra can be interlaced and configurate to minimize the internal stress, thereby producing the miniature multiple-twinned core of **1**.

The ellipsoidal-shaped Ag_{71} core is contained in a barrel of 70 surface Ag atoms (Figure 3c). The latter can be visualized as being constructed by capping the 20 approximately planar ν_2 triangular (light blue in Figure 1b) faces of the former with 60 Ag atoms (three each, forming a ν_1 triangle in the third shell), and 10 slightly concave butterflies (dark blue in Figure 1b) of the former with 10 Ag atoms near the equator. The surface Ag_{70} shell forms 12 pentagonal, 20 triangular, and 40 tetragonal faces. Overall, the 141 silver atoms in the three shells form a prolate ellipsoidal metal framework with D_5 symmetry.

The metal framework is further protected by 40 S-Adms and 12 bromides, giving rise to the formulation of $[Ag_{141}Br_{12}(S\text{-}Adm)_{40}]^{3+}$ (Figure 3d). The 40 thiolates cap 40 tetragonal faces of the Ag_{70} shell, with an average Ag-S bond lengths 2.589 Å, among which 30 thiolates are four-coordinated, and the other 10 are three-coordinated (Figure 3e and S5). Unlike small thiolates, S-Adm is a rigid and bulky ligand, meaning that the surface S-Adm coverage could be very low. Considering that the surface metal accessibility is governed by the tail groups of the surface ligands, we define herein the surface thiolate coverage as the ratio of the number of thiolates to the surface metal atoms to simplify the comparison. The surface thiolate coverage of **1** is ~57%, much smaller than that of Ag nanoparticle containing a similar number of Ag atoms capped by less bulky thiolates. For instance, the Ag_{136} nanoparticle capped with 4-*tert*-butylbenzenethiolate (TBBT) has a high thiolate coverage of ~78% (Table S1).

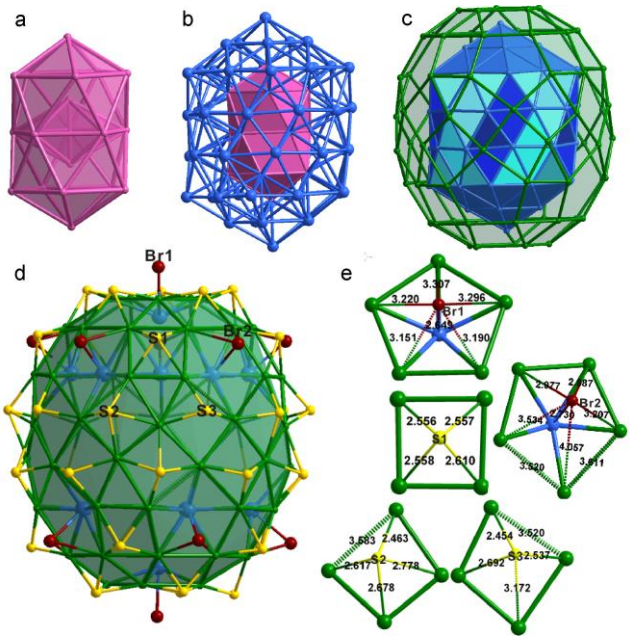

Figure 3. Detailed structure of $[Ag_{141}Br_{12}(S\text{-}Adm)_{40}]^{3+}$. (a) The inner shell of Ag_{19}. (b) The two-shell $Ag_{19}@Ag_{52}$ of the nanoparticle. (c) The three-shell $Ag_{19}@Ag_{52}@Ag_{70}$. (d) Decoration of Ag_{141} with 12 Br (Claret-red) and 40 S (yellow) atoms. (e) Structural details (bond lengths in Å) of the Br and S ligands.

The low coverage of S-Adm on Ag nanoparticles leaves surface sites accessible to small-sized molecules (e.g., halides) (Figure S6). The 12 bromide ligands on **1** are divided into two groups, two at the two poles and ten around the equator (Fig. 3d and 3e). The former forms weak Ag-Br interactions (3.151-3.307 Å) to the pentagonal silver rings. The corresponding distances for the latter range from 2.977- 4.057 Å. However, these bromide ligands also form additional bonds (one each) with the 12 vertices of the Ag_{71} core underneath the pentagonal faces, with Ag-Br bonds of 2.649 Å (two at the poles) and 2.739 Å (average of ten around the equator), respectively (Figure 3e). Experimentally, when PPh_4Br was replaced by PPh_4Cl or PPh_4I in the synthesis, the corresponding $[Ag_{141}X_{12}(S\text{-}Adm)_{40}]^{3+}$ (X=Cl, I) nanoparticles were obtained, as confirmed by ESI-MS (Figure S7 and S8) and single-crystal structure characterization.

The atomic and electronic structure of $[Ag_{141}Br_{12}(S\text{-}Adm)_{40}]^{3+}$ were analyzed with Density Functional Theory (DFT) (see Supporting Information for details). The jelliumatic electron count of **1** gives 86 electrons, given the charge state of +3. This number does not indicate shell closing in a spherical electron system where the typical shell closing electron counts are 2, 8, 18, 20, 34, 40, 58, 68, 70, 92 …. This is expected due to the overall prolate shape of the particle, which splits the degeneracies of angular momentum symmetries. Additional splitting is due to the D_5 symmetry. DFT analysis of the electronic density of states shows that the occupied electron states within 0.4 eV of the highest occupied molecular orbital (HOMO) resemble the spherical symmetries of 2D, 3S and 1H (Figure S9). However, there is a strong splitting of the states below and above the HOMO level (Figure S10). **1** in the charge state of +3 has an empty orbital (2-electron hole) virtually at the HOMO level, followed by an energy gap of close to 0.3 eV to two upper levels that complete the electron filling to the spherical magic number of 92. The existence of the electron holes very close to the HOMO of **1** suggests that the stability of **1** (Figure S11) is mainly due to structural packing of the metal core and bulky ligand shell, instead of electron shell-closing. Moreover, computed optical spectra of **1** in the charge states +3 and +1 agree qualitatively well with the experiment, showing one absorption maximum at 406 nm and 396 nm for the tri- and mono-

cations, respectively (Figure S12). Further analysis (Figure S13) shows that these peaks are plasmonic in nature and can be assigned to, collectively, the transitions over a large number of single-electron/single-hole states. The induced oscillation of the electron density at the plasmon energy extends to the ligand layer.

Together with its well-defined molecular structure, the excellent stability of **1** makes it an ideal system for studying the surface reactivity of multiple-twinned metal nanoparticles. Similar to the substitution of Br^- by Cl^- (Figure 2b), 3 out of 12 iodides in $[Ag_{141}I_{12}(S\text{-}Adm)_{40}]^{3+}$ are substituted by chlorides (from the solvent) under ESI-MS conditions (Figure S8). This can be explained by the relative strengths of Ag-X (halides) bonds that follow the trend of Ag-Cl>Ag-Br>Ag-I and the steric effect caused by the size difference that follow the opposite trend of Cl<Br<I. In other words, the weakest Ag-I bonds are not so easily replaced by Ag-Cl bonds owing to the large size of the iodides that fit snugly in the cavities created by the S-Adm ligands.

To our surprise, when phenylacetylene (PA) was used as the exchange ligand, two $[PA]^-$ replace two $[S\text{-}Adm]^-$ ligands (Figure 4a) instead of substituting halides. This is counterintuitive since Ag-S bonds are much stronger than Ag-X and Ag-C bonds. The answer lies in the particular surface structure of **1** caused by the bulky thiolates. There are 14 longer-than-normal Ag-S bonds in middle layers of **1**. These S atoms (marked in pink in Figure S14) are three-coordinated or four-coordinated. One or two Ag-S bonds among them are longer than 2.7 Å. The longer-than-normal Ag-S bonds make the thiolates easy targets for attack and eventual replacement by PA. Our studies also revealed that S-Adms on middle layers of $[Ag_{141}Cl_{12}(S\text{-}Adm)_{40}]^{3+}$ are easily replaced by *tert*-butyl mercaptan (TBSH). With the increasing ratio of SR : Ag_{141}, the number of substituted S-Adms increases to reach a maximal value of 14. The latter matches perfectly with the 14 thiolate sites on the middle layers of **1.**

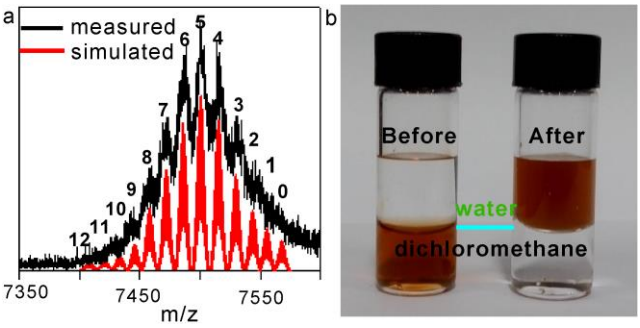

Figure 4. (a) ESI-MS spectra of **1** after ligand-exchange with phenylacetylene (PAH), yielding $[Ag_{141}Br_{12-n}Cl_n(S\text{-}Adm)_{38}PA_2]^{3+}$ (n=0-12). (b) Photographs of the solution of $[Ag_{141}Br_{12}(S\text{-}Adm)_{40}]^{3+}$ before and after ligand-exchange with mercaptosuccinic acid, followed by dissolving in a mixture of dichloromethane and water .

To capitalize on the high surface reactivities of **1**, we also investigated its ligand-exchange behavior with water-soluble mercaptosuccinic acid (MSA).[23-26] In a typical experiment, MSA was added to an ethanol suspension of **1**. After stirring at room temperature for 8h, ammonia was added to deprotonate MSA, resulting in the precipitation of the thiolate-ligand-exchanged Ag nanoparticles. The solid products were separated by centrifugation and washed three times with ethanol. The collected Ag nanoparticles became highly soluble in water (Figure 4b). The aqueous solution of the obtained nanoparticles exhibited practically the same UV-vis spectrum (Figure S16), indicating that the metal core remained intact after the ligand exchange. To achieve the successful transformation of **1** into water soluble, the molar ratio of MSA : **1** used in the ligand exchange can be as low as 4:1 (Figure S17). In comparison, the same ligand exchange process failed to solubilize TBBT-capped $[Ag_{136}(SR)_{64}Cl_3]^-$ in water, even with a MSA : Ag_{136} molar ratio of 12:1 (Figure S18). We believe the reason is that the surface of the latter nanocluster is heavily covered by the less bulky thiolates, rendering it resistant to thiol exchange. These results reinforce the notion that **1** exhibits enhanced surface reactivity towards ligand exchange due to its low surface thiolate coverage.

In summary, this work demonstrated that the use of bulky 1-adamantanethiolate facilitates the formation of a heavily twinned metal nanoparticle, $[Ag_{141}Br_{12}(S\text{-}Adm)_{40}]^{3+}$, with a prolate Ag_{71} core protected by a shell of $Ag_{70}Br_{12}(S\text{-}Adm)_{40}$. Even with twenty v_2 tetrahedral domains, the Ag_{71} core adopts a non-perfect spherical geometry instead of icosahedron, serving as a molecular structure model for multiple-twinned nanostructures of face-center cubic metals. The low surface coverage of bulky thiolates may be related to the multiple-twinned feature of the metal core, suggesting the importance of surface ligands in controlling the shape of metal nanocrystals. Moreover, the low surface thiolate coverage yields high surface reactivities towards ligand exchange. The chemistry behind the controlled formation of heavily-twinned metal nanoparticles with high surface reactivity using bulky ligands is expected to be useful in creating atomically precise metal nanoparticles with desirable surface and/or unusual properties for specific applications.

ASSOCIATED CONTENT

Supporting Information. Experimental details, crystallographic data including the CIF file, computational details, analysis of the electronic structure, mass spectra, and UV-Vis spectra of clusters.

AUTHOR INFORMATION

Corresponding Author

* nfzheng@xmu.edu.cn
* boonkteo@xmu.edu.cn
* hannu.j.hakkinen@jyu.fi

Author Contributions

§L.T.R. and P. Y. contributed equally to this work.

Notes

The authors declare no competing financial interest.

ACKNOWLEDGMENT

We thank the MOST of China (2017YFA0207302, 2015CB932303) and the NSFC of China (21731005, 21420102001, 21333008, 21390390) for financial support. The financial support (to BKT) from iChEM, Xiamen University, and (to HH) from National Innovation and Intelligence Introduction Base program is gratefully acknowledged. The work in University of Jyväskylä was supported by the Academy of Finland (project 294217 and Academy Professorship to H.H.). The computations were made at the CSC computing center in Espoo, Finland.

REFERENCES

(1) Daniel, M.-C.; Astruc, D. *Chem. Rev.* **2004**, *104*, 293.
(2) Liu, P. X.; Qin, R. X.; Fu, G.; Zheng, N. F. *J. Am. Chem. Soc* **2017**, *139*, 2122.
(3) Huang, X. Q.; Tang, S. H.; Mu, X. L.; Dai, Y.; Chen, G. X.; Zhou, Z. Y.; Ruan, F. X.; Yang, Z. L.; Zheng, N. F. *Nat. Nanotech.* **2011**, *6*, 28.
(4) Tao, A. R.; Habas, S.; Yang, P. *Small* **2008**, *4*, 310.
(5) Xia, Y.; Xiong, Y.; Lim, B.; Skrabalak, S. E. *Angew. Chem. Int. Ed.* **2009**, *48*, 60.
(6) Chen, G. X.; Xu, C. F.; Huang, X. Q.; Ye, J. Y.; Gu, L.; Li, G.; Tang, Z. C.; Wu, B. H.; Yang, H. Y.; Zhao, Z. P.; Zhou, Z. Y.; Fu, G.; Zheng, N. F. *Nat. Mater.* **2016**, *15*, 564.
(7) Wu, B. H.; Huang, H. Q.; Yang, J.; Zheng, N. F.; Fu, G. *Angew. Chem. Int. Ed.* **2012**, *51*, 3440.
(8) Song, Y.; Murray, R. W. *J. Am. Chem. Soc* **2002**, *124*, 7096.
(9) Donkers, R. L.; Song, Y.; Murray, R. W. *Langmuir* **2004**, *20*, 4703.
(10) Nel, A. E.; Madler, L.; Velegol, D.; Xia, T.; Hoek, E. M. V.; Somasundaran, P.; Klaessig, F.; Castranova, V.; Thompson, M. *Nat Mater* **2009**, *8*, 543.

(11) Gavia, D. J.; Shon, Y.-S. *Langmuir* **2012**, *28*, 14502.
(12) Jadzinsky, P. D.; Calero, G.; Ackerson, C. J.; Bushnell, D. A.; Kornberg, R. D. *Science* **2007**, *318*, 430.
(13) Zhu, M.; Aikens, C. M.; Hollander, F. J.; Schatz, G. C.; Jin, R. *J. Am. Chem. Soc.* **2008**, *130*, 5883.
(14) Heaven, M. W.; Dass, A.; White, P. S.; Holt, K. M.; Murray, R. W. *J. Am. Chem. Soc.* **2008**, *130*, 3754.
(15) Yang, H. Y.; Wang, Y.; Huang, H. Q.; Gell, L.; Lehtovaara, L.; Malola, S.; Häkkinen, H.; Zheng, N. F. *Nature Commun.* **2013**, *4*, 2422.
(16) Desireddy, A.; Conn, B. E.; Guo, J.; Yoon, B.; Barnett, R. N.; Monahan, B. M.; Kirschbaum, K.; Griffith, W. P.; Whetten, R. L.; Landman, U.; Bigioni, T. P. *Nature* **2013**, *501*, 399.
(17) Dass, A.; Theivendran, S.; Nimmala, P. R.; Kumara, C.; Jupally, V. R.; Fortunelli, A.; Sementa, L.; Barcaro, G.; Zuo, X.; Noll, B. C. *J. Am. Chem. Soc.* **2015**, *137*, 4610.
(18) Yang, H. Y.; Wang, Y.; Chen, X.; Zhao, X. J.; Gu, L.; Huang, H. Q.; Yan, J. Z.; Xu, C. F.; Li, G.; Wu, J. C.; Edwards, A. J.; Dittrich, B.; Tang, Z. C.; Wang, D. D.; Lehtovaara, L.; Häkkinen, H.; Zheng, N. F. *Nature Commun.* **2016**, *7*, 12809.
(19) Jin, R.; Zeng, C.; Zhou, M.; Chen, Y. *Chem. Rev.* **2016**, *116*, 10346.
(20) Yang, H. Y.; Yan, J. Z.; Wang, Y.; Su, H. F.; Gell, L.; Zhao, X. J.; Xu, C. F.; Teo, B. K.; Häkkinen, H.; Zheng, N. F. *J. Am. Chem. Soc.* **2017**, *139*, 31.
(21) Alhilaly, M. J.; Bootharaju, M. S.; Joshi, C. P.; Besong, T. M.; Emwas, A.-H.; Juarez-Mosqueda, R.; Kaappa, S.; Malola, S.; Adil, K.; Shkurenko, A.; Häkkinen, H.; Eddaoudi, M.; Bakr, O. M. *J. Am. Chem. Soc* **2016**, *138*, 14727.
(22) Wang, Y.; Wan, X. K.; Ren, L. T.; Su, H. F.; Li, G.; Malola, S.; Lin, S. C.; Tang, Z. C.; Häkkinen, H.; Teo, B. K.; Wang, Q. M.; Zheng, N. F. *J. Am. Chem. Soc.* **2016**, *138*, 3278.
(23) Warner, M. G.; Reed, S. M.; Hutchison, J. E. *Chem. Mater.* **2000**, *12*, 3316.
(24) Duan, H.; Nie, S. *J. Am. Chem. Soc* **2007**, *129*, 2412.
(25) Udayabhaskararao, T.; Sun, Y.; Goswami, N.; Pal, S. K.; Balasubramanian, K.; Pradeep, T. *Angew. Chem. Int. Ed.* **2012**, *51*, 2155.
(26) Wang, Y.; Su, H.; Xu, C.; Li, G.; Gell, L.; Lin, S.; Tang, Z.; Häkkinen, H.; Zheng, N. *J. Am. Chem. Soc* **2015**, *137*, 4324.

TOC

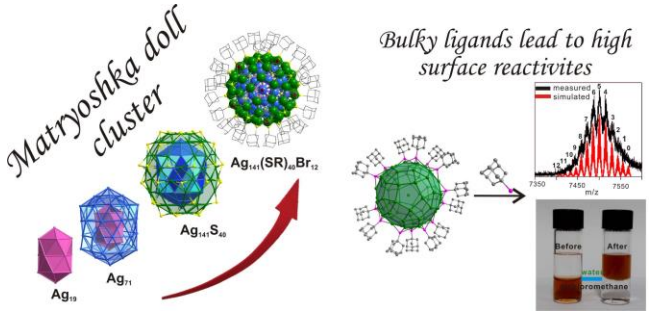
Matryoshka doll cluster
$Ag_{141}(SR)_{49}Br_{12}$
$Ag_{141}S_{49}$
Ag_{71}
Ag_{19}
Bulky ligands lead to high surface reactivites
measured
simulated
m/z
Before
After
water
bromomethane